

Active Role of Oxide Support during CO Oxidation at Au/MgO

L. M. Molina and B. Hammer

iNANO and Department of Physics and Astronomy, University of Aarhus, DK-8000 Aarhus C, Denmark
(Received 29 January 2003; published 23 May 2003)

The oxidation of CO at MgO supported gold aggregates is studied by means of density functional theory calculations. In addition to serving as a structural promoter holding the gold particles, the supporting oxide also takes an active role in the bonding and activation of adsorbates bound to the gold. The oxide stabilizes a peroxolike reaction intermediate, $\text{CO} \cdot \text{O}_2$, and causes steric repulsion to CO. The most reactive site at Au/MgO appears where the gold shelters the MgO thereby creating a cavity where several low-coordinated Au atoms and Mg^{2+} cations from the substrate can interact simultaneously with an adsorbate.

DOI: 10.1103/PhysRevLett.90.206102

PACS numbers: 68.47.Jn, 68.35.Np, 68.43.Fg, 82.65.+r

Heterogeneous catalysts are often realized as small clusters of active material, typically a late transition metal, on an oxide support. The role of the oxide is largely considered that of a structural promoter, which depending on the metal-oxide adhesion energetics [1] assures a large surface area of the active material by supporting many small clusters [2]. The precise cluster size distribution is of great importance for the reactivity of such supported clusters [3]. This applies, in particular, for sub-nm-sized clusters as recently demonstrated by Heiz and co-workers [4] for monodispersed size-selected Rh, Pd, Pt, and Au clusters supported by MgO(100). For these systems finite size effects were identified and explained in terms of electron shell models and charge transfer from the support to the metallic clusters [5].

A particularly interesting active material is gold, which in its bulk form is rather inert to interaction with gasses [6], while it becomes highly reactive in the form of nano-sized clusters. Haruta and co-workers [7] found titania supported gold clusters capable of oxidizing CO at temperatures below 0 °C and subsequent studies have identified a strong dependence of the reactivity on the choice of oxide support and on the cluster size, with general consensus that nm-sized Au clusters exhibit higher reactivity towards CO oxidation than larger clusters—both on reducible [8] and nonreducible oxides (including MgO) [9].

The role of the oxide support has often been speculated to be more than that of a structural promoter. In the reaction kinetics, the spillover effects of reactants moving between the active material and the support is well established [10], but an even more direct role of the support has been suggested to be that of promoting reactions at special sites right at the metal-support interface boundary [11]. In the present Letter, we present a density functional theory (DFT) investigation of this possibility. The system of oxide supported Au clusters is chosen for the study, since the moderate adsorption bonds formed on Au leave room for non-negligible contributions from the support. For the oxide support, MgO(100) is chosen because of its structural simplicity and because of its appearance in the experimental literature. We model the CO oxidation in the

presence of O_2 and find indeed the most reactive gold sites being right at the gold-oxide support interface boundary. The support provides attractive interaction with a peroxo-like reaction intermediate, and repulsive, steric interaction with the CO species.

In order to know how to model the Au-MgO interface, we start by considering how gold clusters form on MgO. Generally, the shape of large metal particles on a support can be predicted from the Wulff-Kaichew construction [12,13]. Depending on the surface energy of the crystal facets and on the adsorption bond strength of molecules from the surrounding gas phase [14], supported clusters in thermodynamical equilibrium form polyhedra that expose only low-index crystal facets. The metal-oxide adhesion energy determines the truncation of the Wulff polyhedra at the interface [15]. For Au on MgO(100), clusters have been observed experimentally to expose Au(100) on the top [16,17], indicating an epitaxial growth. Using DFT (PW91 self-consistent—see below) we calculate a Au(100) surface energy of 0.84 J/m² and a Au-MgO adhesion energy of 0.52 J/m² meaning that the Wulff-Kaichew construction predicts large clusters to assume the partial wetting shape indicated in Fig. 1(a), which is in agreement with the experiments [16,17]. For small gold particles the Wulff-Kaichew construction becomes uncertain, since it neglects the extra formation energy for edge and corner atoms. Consequently, particles wetting the support more than predicted from the Wulff-Kaichew construction might prevail for small clusters. As an example of this, we present in Fig. 1(b) and 1(c) on the basis of our DFT calculations, two relaxed structures of Au₃₄/MgO(100). We find the structure of Fig. 1(b) to be more than 0.10 eV more stable than the Wulff-Kaichew polyhedron like structure of Fig. 1(c). Semiempirical calculations for Pd clusters on MgO [18] also show this behavior, which is further observed in TEM studies of Au particles at anatase TiO₂ [19].

We now investigate how the CO oxidation reaction at gold clusters is affected by the oxide support. Since the Au-MgO interfacial structure depends on the cluster size we choose to work with the three different Au-MgO

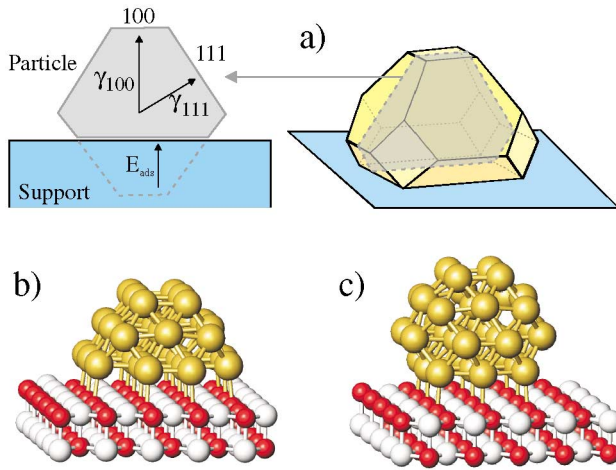


FIG. 1 (color online). (a) Schematic illustration of a truncated Wulff polyhedron on a support. (b),(c) DFT (PW91 self-consistent) derived, relaxed structures of Au_{34} supported on $\text{MgO}(100)$ with a decreasing degree of partial wetting behavior.

interface boundaries shown in Figs. 2(a)–2(c). These structures, referred to below as type I, II, and III, model clusters of increasing size with decreasing degree of partial wetting.

The DFT calculations we perform using ultrasoft pseudopotentials [20] and the spin polarized, nonlocal density gradient approximation (GGA), with a plane-wave basis ($E_{\text{cut}} = 25 \text{ Ry}$) [21]. Below, energetics based on the revised-Perdew-Burke-Ernzerhof (RPBE) GGA functional [22] is discussed since this functional is most reliable for molecular reactions and adsorption energetics [22,23]. In Table I we include for consistency with the literature the energetics based on the Perdew-Wang-91(PW91)-GGA functional [24]. More details on the calculations are given in the table caption.

Included in Figs. 2(a)–2(c) are the CO adsorption configurations determined by the DFT calculations. For the type II and III Au-MgO interfaces a fairly large CO-Au binding energy of about 0.4 eV is found (cf. Table I). The CO is adsorbed in the “equatorial plane” and any inclination out of this plane is found to lead to an energy increase. For the type I Au-MgO interface, CO binds less

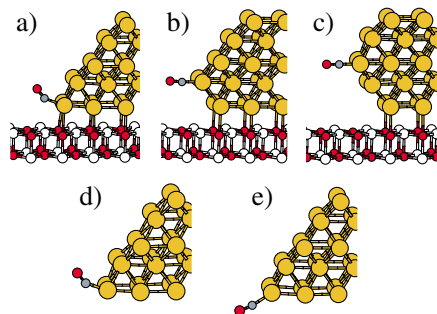


FIG. 2 (color online). (a)–(c) Bonding of CO to type I, II, and III Au-MgO interface boundaries. (d),(e): Removing from (a) the support without and with ionic relaxation.

favorably and attains a bent configuration. The origin of the reduced binding can be unveiled by removing the oxide support for this system as shown in Figs. 2(d) and 2(e). Keeping the configuration fixed, the CO-Au bond is increased by only 0.01 eV, while allowing the CO and Au atoms to relax leads to a further 0.20 eV stabilization. The presence of the oxide support thus sterically hinders the CO from adopting its most stable adsorption configuration, which is comparable in strength to that at the other interfaces. The calculated strong binding at low-coordinated Au atoms agrees well with experimental evidence for edge atoms being the only sites available to CO adsorption on titania supported Au clusters [25] and with the theoretical interpretation that low Au-Au coordination is an important parameter [26,27].

TABLE I. Reaction energetics calculated in the RPBE (PW91) given in eV. The type I, II, and III interfaces are described by two layer $\text{MgO}(100)$ – (5×2) slabs with 22, 26, and 26 Au atoms attached as a one-dimensional gold rod in the y direction. The calculated 4.30 \AA lattice constant of the MgO is employed. A (1×4) \mathbf{k} -point sampling is used. The adsorbate atoms are relaxed together with the nearby 6, 8, and 8 Au atoms. The facets are modeled with unsupported 4 layer $\text{Au}(100)$ – (3×2) and $\text{Au}(111)$ – (2×2) slabs having two layers relaxed and being sampled with (2×3) and (4×4) \mathbf{k} points, respectively. The calculated 4.18 \AA lattice constant is used. The type I-III results are RPBE self-consistent, while the $\text{Au}(100)$ and $\text{Au}(111)$ results are PW91 self-consistent.

	Type I	Type II	Type III	Au(100)	Au(111)
$\text{CO} \rightarrow \text{CO}(a)$					
ΔE	−0.21 (−0.50)	−0.37 (−0.69)	−0.41 (−0.72)	−0.20 (−0.50)	0.02 (−0.26)
$\text{O}_2 \rightarrow \text{O}_2(a)$					
ΔE	0.21 (−0.16)	0.10 (−0.20)	0.09 (−0.19)	0.13 (−0.02)	0.11 (−0.01)
$\text{O}_2 \rightarrow 2\text{O}(a)$					
ΔE	−0.29 (−0.77)	0.19 (−0.40)	0.71 (0.28)	0.97 (0.41)	1.54 (0.97)
$\text{CO}(a) + \text{O}_2 \rightarrow \text{CO} \cdot \text{O}_2(a)$					
ΔE	−0.46 ^a (−1.01) ^a	−0.40 ^b (−0.99) ^b −0.28 ^d (−0.83) ^d	−0.05 ^c (−0.46) ^c 0.14 ^e (−0.56) ^e	0.00 (−0.47)	0.11 (−0.43)
E_a	0.32 ^a (−0.14) ^a	0.50 ^b (0.07) ^b 0.14 ^d (−0.14) ^d	0.28 ^c (−0.01) ^c	0.29 (0.02)	0.35 (0.03)
$\text{CO} \cdot \text{O}_2(a) \rightarrow \text{CO}_2 + \text{O}(a)$					
ΔE	−2.69 (−2.27)	−2.45 ^d (−2.04) ^d	−2.40 (−2.06)	−2.51 (−2.21)	−2.56 (−2.21)
E_a	0.33 (0.34)	0.27 ^d (0.26) ^d	0.24 (0.17)	0.40 (0.40)	0.41 (0.39)

^aFigure 3(a). ^bFigure 3(b). ^cFigure 3(c). ^dFigure 3(d). ^eFigure 3(f).

The next step in the catalytic oxidation of the CO would ordinarily be the dissociative adsorption of O_2 . However, although atomic oxygen shows a moderate binding to gold [28] (cf. Table I), we calculate very high (~ 1 eV) energy barriers for the O_2 dissociation and therefore we exclude such pathways. When CO is already present at the gold surface the situation changes and according to our DFT calculations, a pathway becomes active along which an adsorbed $CO \cdot O_2$ reaction intermediate is formed. Figures 3(a)–3(c) depict this complex in its most stable configuration at the three different Au-MgO interfaces. The adsorbed $CO \cdot O_2$ is characterized by $\sim 120^\circ$ O-C-O and O-C-Au angles and a O-O peroxy bond of about 1.45 Å and zero magnetic moment. During the endothermic O_2 adsorption in the absence of CO, the molecular oxygen attains a superoxo state with a 1.35 Å bond length and a magnetic moment of 0.8.

The finding of the $CO \cdot O_2$ reaction intermediate is in accord with the identification of this very complex

by vibrational spectroscopy for the $CO + O_2$ reaction on gas phase Au monomers [29], with the observation of cooperative CO and O_2 adsorption on various anionic Au clusters [30,31], and with recent theoretical work [32].

The stability of the $CO \cdot O_2$ complexes in Figs. 3(a)–3(c) vary somewhat. On interfaces I and II, the $CO \cdot O_2$ complex is bound very near to the MgO support with a bond strength which is about 0.4 eV more than the binding of the CO alone. On interface III, the complex is adsorbed further from the support and the binding energy only marginally exceeds that of the CO alone. If on interface II the complex is rotated into the configuration depicted in Fig. 3(d), the binding energy reduces by 0.12 eV as the complex-MgO separation increases, but another 0.17 eV is still lost upon completely removing the oxide support as in Fig. 3(e). In Fig. 3(f) the complex is moved closer to the support at interface III, causing a 0.13 eV larger complex-support interaction [calculated from 0.06 and 0.19 eV losses of removing the substrate from Figs. 3(c) and 3(f), respectively], but the binding energy is reduced overall by 0.19 eV, since the low coordinated, equatorial gold atom is no longer involved in the bonding.

To unveil the nature of the attractive complex-support interaction inferred so far from the adsorption energetics, we plot in Figs. 3(g)–3(i) some electron density profiles for the system of $CO \cdot O_2$ at the type II interface, Figs. 3(d) and 3(e). The first two plots show the induced charge density upon introducing the oxide support to either the system of Fig. 3(e) or the system of unsupported clean gold with the type II interface but no adsorbate. Both plots [Figs. 3(g) and 3(h)] show electron transfer from the oxide to the gold and only when subtracting the two, as in Fig. 3(i), the adsorbate-oxide support interaction becomes evident. The charge rearrangement is seen to be largely that of electron accumulation at the peroxy part of the complex. Figure 3(j) shows the same rearrangement for the most stable configuration. In this latter case the charge transfer is slightly larger, in agreement with a shorter distance from the terminal O to the support (2.20 Å O-Mg bond distance, very close to the 2.15 Å O-Mg separation within the oxide). This explains the higher binding of $CO \cdot O_2$ in Fig. 3(b). Based on Figs. 3(i) and 3(j) we assign the $CO \cdot O_2$ -MgO interaction to be of electrostatic character.

The energy barriers for the $CO \cdot O_2$ (a) formation and dissociation reactions are given in Table I and the potential energy diagrams are shown in Fig. 4. Since we find no low barrier pathway into the most stable $CO \cdot O_2$ configuration at interface II, we base the energy diagram for this interface on the second most stable configuration found [Fig. 3(d)]. From Fig. 4 we conclude that type II Au-MgO interfaces by far will be the most reactive type of interface. The type I interfaces suffer from the steric CO repulsion by the oxide support (i) meaning fewer CO molecules will be adsorbed and hence O_2 will be trapped less efficiently. Type III interfaces do bind the

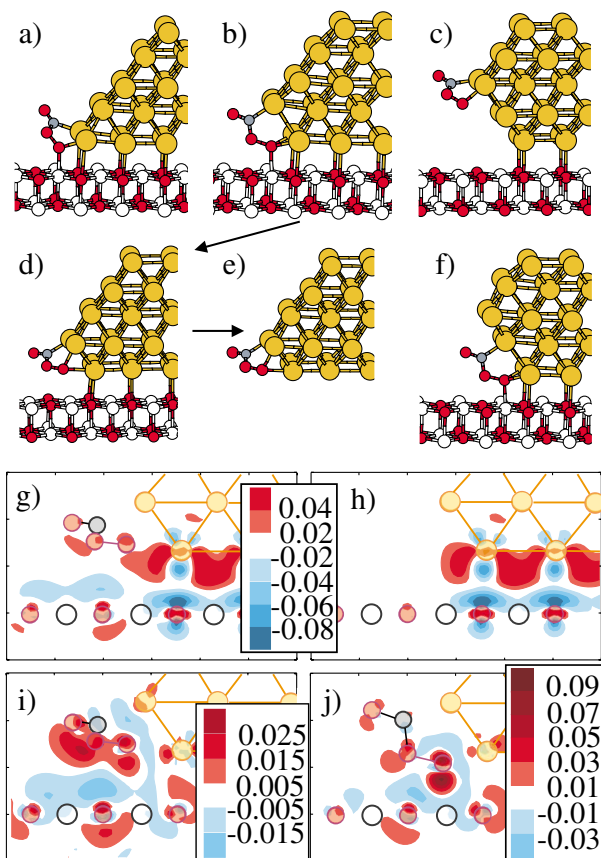


FIG. 3 (color online). (a)–(c) $CO \cdot O_2$ binding configurations at interfaces I, II, and III. (d), (e) Alternative configuration at interface II, with and without the support. (f) $CO \cdot O_2$ at a similar arrangement as in (b), but at interface III. (g)–(i) Induced charge densities (y integrated) for the (d), (e) configuration in units of $e^-/\text{Å}^2$; (g) $\rho_{\text{ads/Au}} = \rho(\text{CO} \cdot \text{O}_2/\text{Au/MgO}) - \rho(\text{CO} \cdot \text{O}_2/\text{Au}) - \rho(\text{MgO})$, (h) $\rho_{\text{Au}} = \rho(\text{Au/MgO}) - \rho(\text{Au}) - \rho(\text{MgO})$, (i) $\rho_{\text{ads/Au}} - \rho_{\text{Au}}$. (j) same as (i) but for configuration (b).

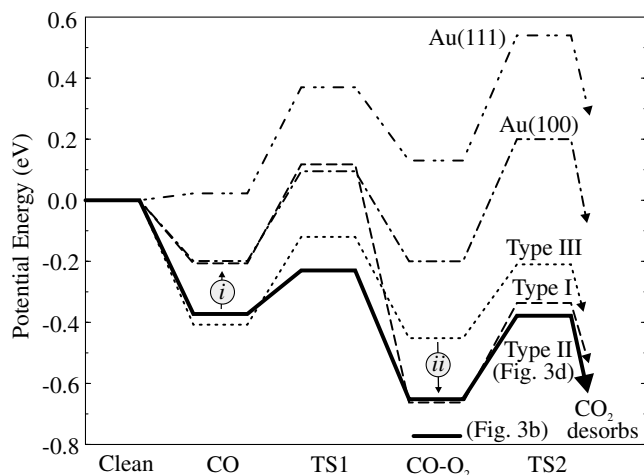


FIG. 4. Calculated RPBE reaction energetics for the $\text{CO} + \text{O}_2 \rightarrow \text{CO}_2 + \text{O}(\text{a})$ reaction.

CO molecules, but lack at their Au edge sites the electrostatic stabilization (ii) of the $\text{CO} \cdot \text{O}_2$ intermediate.

The calculated energy barriers associated with the CO_2 formation on the type II interface are very low, in good agreement with experiments showing the gold clusters to be reactive at room temperature and even below [9]. Since these Au-MgO interfaces are expected to form only for clusters that are not too small (Au_{34} was shown above to have type I interfaces) we note that the present results predict the reactivity per site to go through a maximum as the cluster sizes are reduced, as has been observed to happen for Au/ TiO_2 [8]. Also, this agrees with the finding of larger activity for Au nm-particle catalysts produced using techniques enhancing hemispherical shapes [33].

The reaction site responsible for this maximum reactivity is the small cavity formed between Au and MgO for the type II interface. With combined covalent and ionic interactions between the $\text{CO} \cdot \text{O}_2$, three low-coordinated gold atoms and one substrate Mg^{2+} cation this site is very special—almost looking like the reaction centers in enzymes encountered in biochemistry. The elaborate structure of the reactive site offers a possible reason for the high selectivity found by oxide supported Au clusters for more complicated reactions including propylene epoxidation and hydrogenation of unsaturated hydrocarbons [33].

To complete our investigations of the CO oxidation, we note that the energetics of the $\text{CO} + \text{O}(\text{a}) \rightarrow \text{CO}_2$ reaction is such that any atomically adsorbed oxygen is readily reacted off by CO from the gas phase. The gold clusters will therefore not be polluted by the adsorbed oxygen resulting from the reaction steps of Fig. 4.

Summarizing our DFT calculations, we have shown that the higher reactivity of supported nm-sized Au clusters originates from the presence of two effects, (i) the oxide acts as a structural promoter offering low-

coordinated gold sites, (ii) the oxide interacts with the adsorbates on the gold when these are close enough.

We thank F. Besenbacher and I. Stensgaard for discussions. This work was supported by The Danish Research Councils and Dansk Center for Scientific Computing.

-
- [1] C. T. Campbell, *Surf. Sci. Rep.* **27**, 1 (1997).
 - [2] M. Bäumer and H. J. Freund, *Prog. Surf. Sci.* **61**, 127 (1999).
 - [3] C. R. Henry, *Surf. Sci. Rep.* **31**, 235 (1998).
 - [4] U. Heiz, A. Sanchez, S. Abbet, and W.-D. Schneider, *Chem. Phys.* **262**, 189 (2000).
 - [5] A. Sanchez *et al.*, *J. Phys. Chem. A* **103**, 9573 (1999).
 - [6] B. Hammer and J. K. Nørskov, *Nature (London)* **376**, 238 (1995).
 - [7] M. Haruta, *Catal. Today* **36**, 153 (1997).
 - [8] M. Valden, X. Lai, and D. W. Goodman, *Science* **281**, 1647 (1998).
 - [9] R. J. H. Grisel and B. E. Nieuwenhuys, *J. Catal.* **199**, 48 (2001).
 - [10] R. B. Levy and M. Boudart, *J. Catal.* **32**, 304 (1974).
 - [11] K. Hayek, R. Kramer, and Z. Paal, *Appl. Catal. A* **162**, 1 (1997).
 - [12] G. Wulff, *Z. Kristallogr.* **34**, 449 (1901).
 - [13] W. L. Winterbottom, *Acta Metall.* **15**, 303 (1967).
 - [14] P. L. Hansen *et al.*, *Science* **295**, 2053 (2002).
 - [15] K. H. Hansen *et al.*, *Phys. Rev. Lett.* **83**, 4120 (1999).
 - [16] P. M. Ajayan and L. D. Marks, *Nature (London)* **338**, 139 (1989).
 - [17] S. Giorgio *et al.*, *Philos. Mag. A* **64**, 87 (1991).
 - [18] W. Vervisch, C. Mottet, and J. Goniakowski, *Phys. Rev. B* **65**, 245411 (2002).
 - [19] T. Akita *et al.*, *J. Electron Microsc.* **49**, 657 (2000).
 - [20] D. Vanderbilt, *Phys. Rev. B* **41**, 7892 (1990).
 - [21] M. C. Payne *et al.*, *Rev. Mod. Phys.* **64**, 1045 (1992).
 - [22] B. Hammer, L. B. Hansen, and J. K. Nørskov, *Phys. Rev. B*, **59**, 7413 (1999).
 - [23] S. Kurth, J. P. Perdew, and P. Blaha, *Int. J. Quantum Chem.* **75**, 889 (1999).
 - [24] J. P. Perdew *et al.* *Phys. Rev. B* **46**, 6671 (1992).
 - [25] F. Boccuzzi *et al.* *J. Catal.* **202**, 256 (2001).
 - [26] M. Mavrikakis, P. Stoltze, and J. K. Nørskov, *Catal. Lett.* **64**, 101 (2000).
 - [27] N. López and J. K. Nørskov, *J. Am. Chem. Soc.* **124**, 11 262 (2002)
 - [28] V. A. Bondzie, S. C. Parker, and C. T. Campbell, *Catal. Lett.* **63**, 143 (1999).
 - [29] H. Huber, D. McIntosh, and G. A. Ozin, *Inorg. Chem.* **16**, 975 (1977).
 - [30] W. T. Wallace and R. L. Whetten, *J. Am. Chem. Soc.* **124**, 7499 (2002).
 - [31] J. Hagen *et al.*, *Phys. Chem. Chem. Phys.* **4**, 1707 (2002).
 - [32] Z.-P. Liu and P. Hu, *J. Am. Chem. Soc.* **124**, 14 770 (2002).
 - [33] M. Haruta, *CATTECH* **6**, 102 (2002).